

## WEIBEL INSTABILITY AND ASSOCIATED STRONG FIELDS IN A FULLY 3D SIMULATION OF A RELATIVISTIC SHOCK

K.-I. NISHIKAWA<sup>1</sup>, J. NIEMIEC<sup>2</sup>, P.E. HARDEE<sup>3</sup>, M. MEDVEDEV<sup>4</sup>,  
H. SOL<sup>5</sup>, Y. MIZUNO<sup>1</sup>, B. ZHANG<sup>6</sup>, M. POHL<sup>7</sup>, M. OKA<sup>1</sup>, D. H. HARTMANN<sup>8</sup>

*submitted to ApJL*

### ABSTRACT

Plasma instabilities (e.g., Buneman, Weibel and other two-stream instabilities) excited in collisionless shocks are responsible for particle (electron, positron, and ion) acceleration. Using a new 3-D relativistic particle-in-cell code, we have investigated the particle acceleration and shock structure associated with an unmagnetized relativistic electron-positron jet propagating into an unmagnetized electron-positron plasma. The simulation has been performed using a long simulation system in order to study the nonlinear stages of the Weibel instability, the particle acceleration mechanism, and the shock structure. Cold jet electrons are thermalized and slowed while the ambient electrons are swept up to create a partially developed hydrodynamic (HD) like shock structure. In the leading shock, electron density increases by a factor of  $\lesssim 3.5$  in the simulation frame. Strong electromagnetic fields are generated in the trailing shock and provide an emission site. We discuss the possible implication of our simulation results within the AGN and GRB context.

*Subject headings:* relativistic jets: Weibel instability - shock formation - electron-positron plasma, particle acceleration, magnetic field generation - particle-in-cell

### 1. INTRODUCTION

Particle-in-cell (PIC) simulations can shed light on the microphysics within relativistic shocks. Recent PIC simulations show that particle acceleration occurs within the downstream jet (e.g., Frederiksen et al. 2004; Nishikawa et al. 2003, 2005, 2006, 2008, 2009; Hededal et al. 2004; Hededal & Nishikawa 2005; Silva et al. 2003; Jaroschek et al. 2005; Chang, Spitkovsky & Arons 2008; Dieckmann, Shukla, & Drury 2008; Spitkovsky 2008a,b; Martins et al. 2009). In general, these simulations confirm that a relativistic shock in weakly or non magnetized plasma is dominated by the Weibel instability (Weibel 1959). The associated current filaments and magnetic fields (e.g., Medvedev & Loeb 1999) accelerate electrons (e.g., Nishikawa et al. 2006) and cosmic rays, which affect the pre-shock medium (Medvedev & Zakutnyaya 2009).

In this paper we present new three-dimensional simulation results for an electron-positron jet injected into an electron-positron plasma using a long simulation grid. A leading and trailing shock system develops with strong electromagnetic fields accompanying the trailing shock.

<sup>1</sup> Center for Space Plasma and Aeronomic Research, University of Alabama in Huntsville, NSSTC, 320 Sparkman Drive, Huntsville, AL 35805; ken-ichi.nishikawa-1@nasa.gov

<sup>2</sup> Institute of Nuclear Physics PAN, ul. Radzikowskiego 152, 31-342 Kraków, Poland

<sup>3</sup> Department of Physics and Astronomy, The University of Alabama, Tuscaloosa, AL 35487

<sup>4</sup> Department of Physics and Astronomy, University of Kansas, KS 66045

<sup>5</sup> LUTH, Observatoire de Paris-Meudon, 5 place Jules Jansen, 92195 Meudon Cedex, France

<sup>6</sup> Department of Physics, University of Nevada, Las Vegas, NV 89154

<sup>7</sup> Department of Physics and Astronomy, Iowa State University, Ames, IA 50011

<sup>8</sup> Department of Physics and Astronomy, Clemson University, Clemson, SC 29634

### 2. SIMULATION SETUP

The code used in this study is an MPI-based parallel version of the relativistic electromagnetic particle (REMP) code TRISTAN (Buneman 1993; Nishikawa et al. 2003, Niemiec et al. 2008). The simulations have been performed using a grid with  $(L_x, L_y, L_z) = (4005, 131, 131)$  cells and a total of  $\sim 1$  billion particles (12 particles/cell/species for the ambient plasma) in the active grid. The electron skin depth,  $\lambda_s = c/\omega_{pe} = 10.0\Delta$ , where  $\omega_{pe} = (e^2 n_a / \epsilon_0 m_e)^{1/2}$  is the electron plasma frequency and the electron Debye length  $\lambda_D$  is half of the cell size,  $\Delta$ . This computational domain is six times longer than in our previous simulations (Nishikawa et al. 2006; Ramirez-Ruiz, Nishikawa & Hededal 2007). The jet-electron number density in the simulation reference frame is  $0.676 n_a$ , where  $n_a$  is the ambient electron density, and the jet Lorentz factor is  $\gamma_j = 15$ . The jet-electron/positron thermal velocity is  $v_{j,th} = 0.014 c$  in the jet reference frame, where  $c = 1$  is the speed of light. The electron/positron thermal velocity in the ambient plasma is  $v_{a,th} = 0.05 c$ . As in our previous work (e.g., Nishikawa et al. 2006) the jet is injected in a plane across the computational grid located at  $x = 25\Delta$  in order to eliminate effects associated with the boundary at  $x = x_{min}$ . Radiating boundary conditions are used on the planes at  $x = x_{min}$  and  $x = x_{max}$  and periodic boundary conditions on all transverse boundaries (Buneman 1993).

The jet makes contact with the ambient plasma at a 2D interface spanning the computational domain. Here the formation and dynamics of a small portion of a much larger shock are studied in a spatial and temporal way that includes the spatial development of nonlinear saturation and dissipation from the injection point to the jet front defined by the fastest moving jet particles.

### 3. SIMULATION RESULTS

Figure 1a & b show the averaged (in the  $y-z$  plane) (a) jet (red), ambient (blue), and total (black) electron density and (b) electromagnetic field energy divided by the total jet kinetic energy ( $E_t^j = \sum_{i=e,p} m_i c^2 (\gamma_j - 1)$ ) at  $t = 3250 \omega_{pe}^{-1}$ . Here, “e” and “p” denote electron and positron. Positron density profiles are similar to electron profiles. Ambient particles become swept up after jet

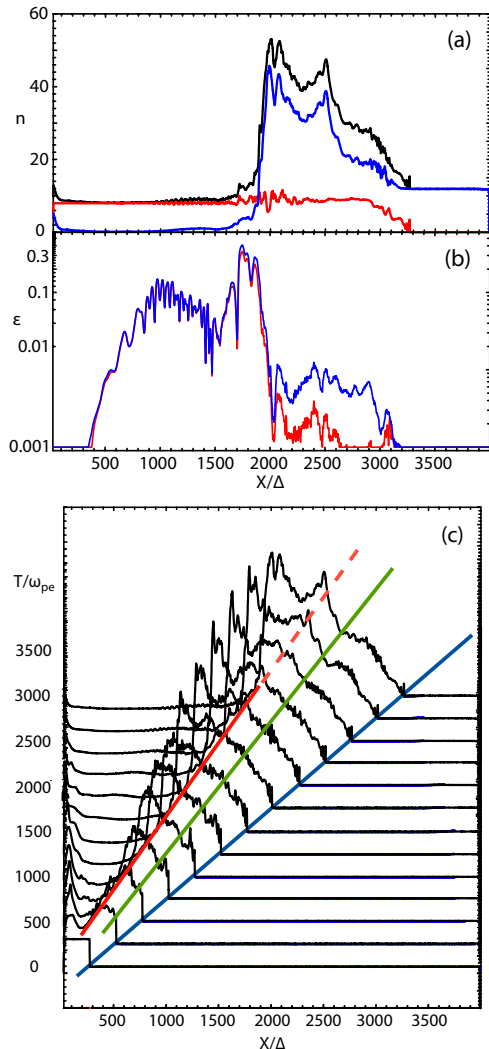


FIG. 1.— Averaged values of (a): jet (red), ambient (blue), and total (black) electron density, and (b): electric (red) and magnetic (blue) field energy divided by the jet kinetic energy at  $t = 3250 \omega_{pe}^{-1}$ . Panel (c) shows the evolution of the total electron density in time intervals of  $\delta t = 250 \omega_{pe}^{-1}$ . Diagonal lines indicate motion of the jet front (blue:  $\lesssim c$ ), predicted contact discontinuity speed (green:  $\sim 0.76 c$ ), and trailing density jump (red:  $\sim 0.56 c$ ).

electrons pass  $x/\Delta \sim 500$ . By  $t = 3250 \omega_{pe}^{-1}$ , the density has evolved into a two-step plateau behind the jet front. The maximum density in this shocked region is about three times the initial ambient density. The jet-particle density remains nearly constant up to near the jet front.

Current filaments and strong electromagnetic fields accompany growth of the Weibel instability in the trailing shock region. The electromagnetic fields are about

four times larger than that seen previously using a much shorter grid system ( $L_x = 640\Delta$ ). At  $t = 3250 \omega_{pe}^{-1}$ , the electromagnetic fields are largest at  $x/\Delta \sim 1700$ , and decline by about one order of magnitude beyond  $x/\Delta = 2300$  in the shocked region (Nishikawa 2006; Ramirez-Ruiz, Nishikawa & Hededal 2007).

Figure 1c shows the total electron density plotted at time intervals of  $\delta t = 250 \omega_{pe}^{-1}$ . The jet front propagates with the initial jet speed ( $\lesssim c$ ). Sharp RMHD-simulation shock surfaces are not created (e.g., Mizuno et al. 2009). A leading shock region (linear density increase) moves with a speed between the fastest moving jet particles  $\lesssim c$  and a predicted contact discontinuity speed of  $\sim 0.76 c$  (see §4). A contact-discontinuity region consisting of mixed ambient and jet particles moves at a speed between  $\sim 0.76 c$  and the trailing density jump speed  $\sim 0.56 c$ . A trailing shock region moves with speed  $\lesssim 0.56 c$ , note the modest density increase just behind the large trailing density jump.

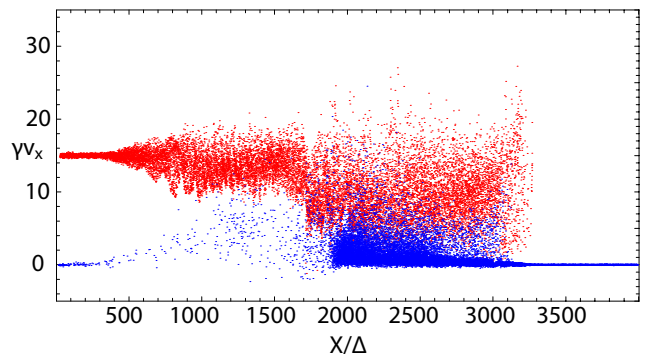


FIG. 2.— Phase-space distribution of jet (red) and ambient (blue) electrons at  $t = 3250 \omega_{pe}^{-1}$ . About 18,600 electrons of both species are selected randomly.

Figure 2 shows the phase-space distribution of jet (red) and ambient (blue) electrons at  $t = 3250 \omega_{pe}^{-1}$  and confirms our shock-structure interpretation. The electrons injected with  $\gamma_j v_x \sim 15$  become thermalized due to Weibel instability-induced interactions. The swept-up ambient electrons (blue) are heated by interaction with jet electrons. Some ambient electrons are strongly accelerated.

Figure 3 shows the velocity distribution of all jet and ambient electrons in the simulation frame. The small peak indicates electrons injected at  $\gamma_j = 15$ . Jet electrons are accelerated to a non-thermal distribution. Ambient electrons are also accelerated to speeds above the jet injection velocity. The velocity distributions of jet and ambient electrons near the jet front (at  $x/\Delta > 2300$ ) are also plotted. The fastest jet electrons,  $\gamma > 20$ , are located near the jet front. On the other hand, the fastest ambient electrons are located farther behind the jet front (at  $x/\Delta < 2300$ ). Thus, strong acceleration of the ambient electrons accompanies the strong fields associated with the Weibel instability.

#### 4. DISCUSSION

Our collisionless-shock structure can be compared to 1-D hydrodynamic (HD) shock predictions (e.g., Blandford & McKee 1976; Zhang & Kobayashi 2005). The

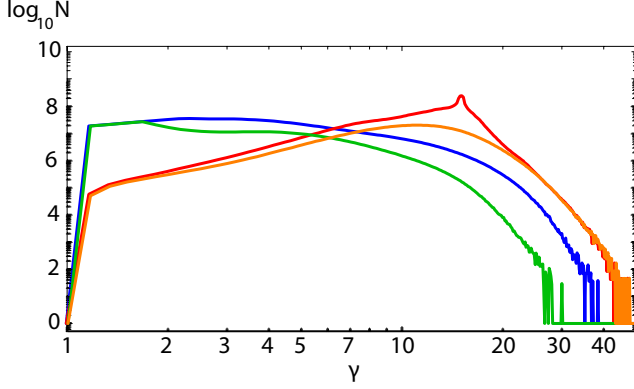


FIG. 3.— Velocity distributions at  $t = 3250 \omega_{pe}^{-1}$ . All jet (red) and all ambient (blue), and at  $x/\Delta > 2300$  jet (orange) and ambient (green) electrons are also plotted. The small (red) peak indicates jet electrons injected at  $\gamma_j = 15$ .

speed of the contact discontinuity (**CD**) is given by ram pressure balance in the CD frame. Our initial conditions allow us to set the total energy density  $e \equiv \rho c^2 + p/(\Gamma - 1) = \rho c^2$  and pressure  $p = 0$ , so that the speed in the ambient frame becomes (Rosen et al. 1999)

$$\beta_{cd} = [(\gamma_j \eta^{1/2})/(\gamma_j \eta^{1/2} + 1)]\beta_j, \quad (1)$$

where  $\eta \equiv \rho_j/\rho_a (= m_e n_j/m_e n_a)$  and mass densities are determined in the “jet” and “ambient” proper frames. In the simulation  $n_j = 0.0451 n_a$  and  $\gamma_j = 15$ , and  $\beta_{cd} = 0.759$  ( $\gamma_{cd} = 1.54$ ) is the predicted CD speed. Formally this should represent the average speed of particles in the CD region.

The leading shock moves at a speed given by

$$\gamma_{ls}^2 = \frac{(\gamma_{cd} + 1)[\Gamma_{sa}(\gamma_{cd} - 1) + 1]^2}{\Gamma_{sa}(2 - \Gamma_{sa})(\gamma_{cd} - 1) + 2} \quad (2)$$

where  $5/3 > \Gamma_{sa} > 4/3$  is the shocked ambient adiabatic index. Thus the leading shock speed is predicted to be  $0.865 > \beta_{ls} > 0.783$  ( $2 > \gamma_{ls} > 1.6$ ) where upper and lower limits correspond to upper and lower limits of  $\Gamma_{sa}$ , respectively.

The jump condition at the leading shock is

$$\frac{n_{sa}}{n_a} = \frac{\Gamma_{sa} \gamma_{cd} + 1}{\Gamma_{sa} - 1}, \quad (3)$$

where  $n_{sa}$  is the shocked ambient density in the proper (CD) frame and we find  $5.34 n_a < n_{sa} < 9.15 n_a$ , where the lower and upper limits correspond to the upper and lower limits to  $\Gamma_{sa}$ , respectively. Measured in the ambient (simulation) frame the shocked ambient density should be  $8.2 n_a < \gamma_{cd} n_{sa} < 14.1 n_a$ . Formally this should represent the total density of particles in the shocked-ambient region.

Computations associated with the trailing shock are most easily performed in the jet rest frame designated below as the “primed” frame. In this frame the CD moves with speed  $\beta'_{cd} = -(\beta_j - \beta_{cd})/(1 - \beta_j \beta_{cd}) = -0.984$  and  $\gamma'_{cd} = 5.60$ . The speed of the trailing shock in the jet frame,  $\gamma'_{ts}$  is given by eq. (2) but with  $\gamma_{cd} \rightarrow \gamma'_{cd}$  and  $\Gamma_{sa} \rightarrow \Gamma_{sj}$  where  $\Gamma_{sj}$  is the shocked-jet adiabatic index. In the jet frame  $10.4 > \gamma'_{ts} > 7.4$  and  $0.995 > -\beta'_{ts} > 0.991$ , where upper and lower limits correspond to upper  $\Gamma_{sj} = 5/3$  and lower  $\Gamma_{sj} = 4/3$  limits to  $\Gamma_{sj}$ , respectively. The

trailing shock speed in the ambient (simulation) frame is  $0.35 < \beta_{ts} = (\beta_j - \beta'_{ts})/(1 - \beta_j \beta'_{ts}) < 0.61$  where the lower and upper limits correspond to the upper and lower limits of  $\Gamma_{sj}$ , respectively.

The density jump at the trailing shock is given by eq. (3) but with  $\gamma_{cd} \rightarrow \gamma'_{cd}$  and  $\Gamma_{sa} \rightarrow \Gamma_{sj}$  where now  $n_{sa}/n_a \rightarrow n_{sj}/n_j$  where  $n_j = 0.0451 n_a$  with result that the proper density of shocked jet material is  $0.70 n_a < n_{sj} < 1.15 n_a$  where lower and upper limits correspond to upper and lower limits to  $\Gamma_{sj}$ , respectively. In the ambient (simulation) frame the shocked jet density should be  $1.08 n_a < \gamma_{cd} n_{sj} < 1.76 n_a$ . Formally this should represent the total density of particles in the shocked jet region.

In the simulation the speed of the trailing density jump is  $\sim 0.56 c$ , which is in the predicted range  $0.35 < \beta_{ts} < 0.61$ , a typical speed within the density-plateau region,  $\sim 0.75 c$ , is close to  $\beta_{cd} = 0.76$ . The poorly defined leading shock structure moves at a speed between  $\sim 0.76 c$  and  $\lesssim c$ , consistent with the predicted  $0.78 < \beta_{ls} < 0.86$ .

In the simulation the maximum density increase observed in the ambient (simulation) frame is  $\gamma_{cd} n_{sa}/n_a \sim 3.5$  behind the leading shock (see Fig. 1a). This is about a factor of  $\sim 3$  smaller than the predicted increase,  $8.2 < \gamma_{cd} n_{sa}/n_a < 14.1$ , for a fully-developed leading shock. On the other hand, the density increase observed in the ambient (simulation) frame of  $\gamma_{cd} n_{sj}/n_a \gtrsim 1$  just before the trailing large density jump is comparable to that predicted,  $1.08 < \gamma_{cd} n_{sj}/n_a < 1.76$ , for a fully developed trailing shock.

Our present results can be compared to those found in the 2-D simulations of Chang et al. (2008) (see also Spitkovsky 2008a). Their simulations were performed in the **CD** frame, and material with proper density,  $n$ , moved into the contact discontinuity with a Lorentz factor  $\gamma = 15$ . A shock moved away from the CD with the predicted speed

$$\beta_s = (\Gamma_s - 1) \left[ \frac{\gamma - 1}{\gamma + 1} \right]^{1/2} = 0.47, \quad (4)$$

and predicted density jump

$$\frac{n_s}{\gamma n} = \frac{1}{\gamma} \frac{\Gamma_s \gamma + 1}{\Gamma_s - 1} = 3.13, \quad (5)$$

for a shocked adiabatic index of  $\Gamma_s = 3/2$ .

In our simulation we have two shocks that move away from the CD. For our leading shock, the ambient plasma moves relative to the CD at a speed equal to  $\beta_{cd} = 0.759$  and  $\gamma = \gamma_{cd} = 1.54$  in eqs. 4 & 5. In the CD frame  $\beta_s = 0.23$  and the observed density jump becomes  $n_{sa}/\gamma_{cd} n_a = 4.3$  for  $\Gamma_s = 3/2$ . So we see that our leading shock speed would be about 50% less than that in Chang et al. (2008) and our density increase would be about 50% larger for a fully-developed leading shock in the CD frame. For the trailing shock, the jet moves toward the CD at a speed equal to  $-\beta'_{cd} = 0.984$  and  $\gamma = \gamma'_{cd} = 5.60$  in eqs. 4 & 5. In the CD frame  $\beta_s = 0.417$  and the observed density increase becomes  $n_{sj}/\gamma'_{cd} n_j = 3.36$  for  $\Gamma_s = 3/2$ . So we see that our trailing shock speed would be about 11% less than that in Chang et al. (2008) and our density increase would be about 7% larger for the fully developed trailing shock in the CD frame. The parameters associated with our trailing shock are similar to those found in Chang et

al. (2008), and the Weibel filamentation structures are comparable but now studied in full 3-D.

## 5. CONCLUSION

The present simulation finds for the first time a relativistic shock system comparable to a predicted relativistic HD shock system consisting of leading and trailing shocks separated by a contact discontinuity, albeit not yet fully developed. One remarkable aspect of this shock system lies in the generation of large electromagnetic fields, up to 30% of the kinetic energy density, associated with the trailing shock. Electromagnetic fields in the leading shock and contact-discontinuity region are over one order of magnitude lower. The large value for  $\epsilon_B \sim 0.3$  in our trailing shock hints that Poynting-flux-dominated ejecta may not be required to explain some GRB observations (McMahon et al. 2006).

Visualization of our dual shock system in the ambient (simulation) frame provides a picture of the shock structure that should exist at the head of a relativistic astrophysical jet,  $\gamma_{jt} = 15$ , that is less dense than the surrounding medium,  $n_{jt}/n_{am} = 0.045$ . Within the AGN context, here we identify our trailing shock with the “jet” shock that decelerates the relativistic jet and we would expect synchrotron emission to originate from the strongly magnetized structure. Little synchrotron emission would originate from the weakly magnetized “bow” shock in front of the contact discontinuity. This in fact is what is observed at the leading edge of extra-galactic jets where synchrotron emission from the bow shock is not typically observed.

Visualization of our dual shock system in the “jet”

frame provides a picture of the shock structure that would accompany a relativistic blast wave driven by relativistic ejecta. Within the GRB context, here we identify the ambient medium as representing relativistic ejecta moving at  $\gamma_{ej} = 15$  into a much less dense ISM,  $n_{ej}/n_{ism} = 22$ . Our trailing shock is now identified with the “forward” shock and we would expect synchrotron emission from this strongly magnetized structure. Little synchrotron emission would originate from the low Lorentz factor, weakly-magnetized “reverse” shock moving back into the ejecta.

Our present simulation involves an electron-positron jet and ambient medium. We might expect similar shock-structure development in electron-ion simulations, albeit on much longer temporal and spatial scales.

This work is supported by AST-0506719, AST-0506666, NASA-NNG05GK73G, NNX07AJ88G, NNX08AG83G, NNX08AL39G, and NNX09AD16G. JN is supported by MNI SW research project N N203 393034, and The Foundation for Polish Science through the HOMING program, which is supported by a grant from Iceland, Liechtenstein, and Norway through the EEA Financial Mechanism. Simulations were performed at the Columbia facility at the NASA Advanced Supercomputing (NAS) and Cobalt at the National Center for Supercomputing Applications (NCSA) which is supported by the NSF. Part of this work was done while K.-I. N. was visiting The Observatoire de Paris, Meudon in summer of 2008. Support from the French Natural Science Research Council is gratefully acknowledged.

## REFERENCES

- Blandford, R.D. & McKee, C.F. 1976, *Phys. Fluids*, 19, 1130  
 Buneman, O., 1993, *Tristan*, in *Computer Space Plasma Physics: Simulation Techniques and Software*, edited by H. Matsumoto Matsumoto & Y. Omura, p. 67, Terra Scientific Publishing Company, Tokyo  
 Chang, P., Spitkovsky, A., & Arons, J. 2008, *ApJ*, 674, 378  
 Dieckmann, M.E., Shukla, P.K. & Drury, L.O.C. 2008, *ApJ*, 675, 586  
 Frederiksen, J.T., Hededal, C.B., Haugbølle, T., & Nordlund, Å. 2004, *ApJ*, 608, L13  
 Hededal, C.B. and Nishikawa, K.-I. 2005, *ApJ*, 623, L89  
 Jaroschek, C.H., Lesch, H., & Treumann, R.A. 2005, *ApJ*, 618, 822  
 Martins, S. F., Fonseca, R. A., Silva, L. O., & Mori, W. B. 2009, *ApJL*, in press  
 McMahon, E., Kumar, P., & Piran, T. 2006, *MNRAS*, 366, 575  
 Medvedev, M.V. & Loeb, A. 1999, *ApJ*, 526, 697  
 Medvedev, M.V. & Zakutnyaya, O.V. 2009, *ApJ*, accepted, (arXiv:0812.1906)  
 Mizuno, Y., Zhang, B., Giacomazzo, B., Nishikawa, K.-I., Hardee, P., Nagataki, S., & Hartmann, D.H., 2009, *ApJ*, 690, 47L  
 Niemiec, J., Pohl, M., Stroman, T. & Nishikawa, K.-I. 2008, *ApJ*, 684, 1174  
 Nishikawa, K.-I., Hardee, P., Richardson, G., Preece, R., Sol, H., & Fishman, G.J. 2003, *ApJ*, 595, 555  
 Nishikawa, K.-I., Hardee, P., Richardson, G., Preece, R., Sol, H., & Fishman, G.J. 2005, *ApJ*, 622, 927  
 Nishikawa, K.-I., Hardee, P., Hededal, C.B., & Fishman, G.J. 2006, *ApJ*, 642, 1267  
 Nishikawa, K. -I., Niemiec, J., Sol, H., Medvedev, M., Zhang, B., Nordlund, A., Frederiksen, J.T., Hardee, P., Mizuno, Y., Hartmann, D.H., & Fishman, G.J., 2008, *AIPCS*, submitted (arXiv:astro-ph/0809.5067)  
 Nishikawa, K. -I., Medvedev, M., Zhang, B., Hardee, P., Niemiec, J., Nordlund, A., Frederiksen, J.T., Mizuno, Y., Sol, H., & Fishman, G.J., 2009, *AIPCS*, submitted (arXiv:astro-ph/0901.4058)  
 Ramirez-Ruiz, E., Nishikawa, K.-I., & Hededal, C.B., 2007, *ApJ*, 671, 1877  
 Rosen, A., Hughes, P.A., Duncan, G.C., Hardee, P.E., 1999, *ApJ*, 516, 729  
 Silva, L.O., Fonseca, R.A., Tonge, J.W., Dawson, J.M., Mori, W.B., & Medvedev, M.V., 2003, *ApJ*, 596, L121  
 Spitkovsky, A. 2008a, *ApJ*, 673, L39  
 Spitkovsky, A. 2008b, *ApJ*, 682, L5  
 Weibel, E.S. 1959, *Phys. Rev. Lett.*, 2, 83  
 Zhang, B. & Kobayashi, S. 2005, *ApJ*, 628, 315